Original Article

Histological Effects of Gold Nanoparticles on the Lung Tissue of Adult Male Albino Rats

Reda H. Elbakary, Ebtsam F. Okasha, Ayah Mohamed Hassan Ragab[1], Mohamed Hassan Ragab[2]

Departments of Histology and [2]Anatomy, Faculty of Medicine, Tanta University, Tanta, [1]Department of Reproductive Health and Family Planning, National Research Centre, Giza, Egypt

Abstract

Short Introduction: Nanoparticles (NPs) represent a new line in the investigations and treatment of group of diseases. Furthermore, it is found in many products and enters the body by different roots as ingestion and inhalation. Lung is more liable to exposure to these particles. Safety of these particles on the lung needs to be examined. **Aim of the Work:** To study the effect of gold NPs (GNPs) on the histological structure of the lung tissue. **Materials and Methods:** Thirty-six healthy male albino rats were randomly divided into three groups including control group (Group I) and two GNP-treated groups (Group II received low dose and Group III received high dose daily for 14 days). At the end of the experiment, all the rats were sacrificed; lungs were dissected and processed to be examined by light and electron microscopy. **Results:** GNPs induced inflammatory infiltration dilatation and congestion of the blood vessels in association with the collapse of lung alveoli and extravasations of red blood cells. Caspase-3 immunohistochemical reaction showed strong positive reaction in Group III mainly. Ultrastructure observation revealed affection of type II pneumocyte and thickening in the alveolar wall. **Conclusions:** GNPs led to histological changes in the lung tissue.

Keywords: Gold nanoparticles, lung, rat

Introduction

Nanotechnology is a promising field for the diagnosis and treatment of a variety of diseases.[1] Human skin biopsies taken from areas of prolonged contact with gold, such as rings, showed the presence of the metal in the tissue. This finding confirmed absorption of the metal even though intact skin.[2]

Nanomaterials can affect health through consumer products and occupational and environmental exposures.[3] Nanoparticles (NPs) were found in many products such as cosmetics, food packaging, beverages, toothpaste, automobiles, and air handling units. In addition, many new nanogold-based biomedical products are being developed for drug delivery, in the treatment of rheumatoid arthritis, for photodynamic therapy of cancer and as antimicrobial agents. Furthermore, it can be used as diagnostic devices for some diseases.[4,5]

NPs enter the body via different ways as ingestion, inhalation, and contact with the body surfaces. Gold has been considered an inert, noble metal with some therapeutic and medicinal value. Hence, it may be relatively noncytotoxic. Various shapes of these particles can easily be obtained from gold. Its ability for conjugation with peptides and proteins can target the gold NPs (GNPs) to specific interaction partners. From this point, gold is the most suitable metal for nanotechnology.[6,7]

One of the most affected organs for local and systemic drug delivery is the lungs because of their large surface area and close contact to the blood circulation. The lungs are also likely to be a major route of occupational or environmental exposure to many engineered NPs.[8] Therefore, it is important to investigate the effects of these NPs on the lung to gain better understanding of particle-related health risks.

Materials and Methods

Preparation of gold nanoparticles

The preparation of GNPs followed the standard citrate reduction route using the modifications of Turkevich protocol.[9,10] Gold

Access this article online

Quick Response Code:

Website: http://www.jmau.org/

DOI: 10.4103/JMAU.JMAU_25_18

Address for correspondence: Dr. Reda H. Elbakary, Department of Histology, Faculty of Medicine, Tanta University, Tanta, Egypt.
E-mail: redahassan99@gmail.com

How to cite this article: Elbakary RH, Okasha EF, Hassan Ragab AM, Ragab MH. Histological effects of gold nanoparticles on the lung tissue of adult male albino rats. J Microsc Ultrastruct 2018;6:116-22.

salt weight of 0.1699 g (HAuCL4) was added to 100 ml of water to form solution. Then the solution was boiled for 45 min. One milliliter of this solution was transferred to 18 ml of the double distilled water in a conical flask for heating and stirred vigorously; when its temperature reached to the boiling point, 1 ml of 0.5% sodium citrate as a reducing agent was quickly added. The color of the solution gradually changed from the initial faint yellow to clear, gray, purple, and tantalizing wine red color of GNPs solution. Heating continued for another 15 min; after that, the solution was removed from the heater, was stirred for further 15 min, and was stored at 4°C to prevent aggregation. This method produces monodisperse spherical GNPs in the range of 10–20 nm in diameter.

Animals

Thirty-six adult male albino rats weighing 180–200 g were used in this study. Animals were housed in clean properly ventilated cages under the same environmental conditions and fed on a standard laboratory diet (in Animal House, National Research Center, Egypt).

Control group, Experimental group I and experimental group II

Rats were randomly divided into three groups, 12 rats per each:

- Control group: animals of this group were kept without any treatment throughout the whole period of the experiment
- Experimental Group I (low-dose GNPs): The animals of this group received (40 μg/kg) GNPs[11] orally by a gastric tube once per day for 14 days
- Experimental group II (high-dose GNPs): The animals of this group received (400 μg/kg) GNPs[11] orally once per day for 14 days.

The animals were sacrificed on the next day at the end of the dosing period, and then the lungs of each animal were dissected.

Histological study

Immediately after the rats were killed, a median sternotomy was performed. Lungs were removed from the thoracic cavity; portions of the lung from each rat were cut rapidly and fixed. Paraffin-embedded sections (5 μm) were stained with hematoxylin and eosin (H and E)[12] and examined under a light microscope.

Immunohistochemical study

Expressions of activated caspase-3 were studied. Deparaffinized sections were hydrated, treated with trypsin solution for 15 min at 37°C for antigen retrieval, and then treated with 3% hydrogen peroxide solution in methanol for 10 min to block endogenous peroxidase activity. These steps were followed by washing the sections in phosphate buffered saline (PBS) and subsequently incubating for 10 min at room temperature with 10% goat serum to block unspecific binding. The sections were incubated overnight at 4°C with the specific primary antibody diluted in PBS. They were then washed in PBS and incubated at room temperature for 30 min with specific secondary antibody. The sections were then washed in PBS, revealed by treating with liquid diaminobenzidine, and then counterstained with hematoxylin. Negative control was done by exclusion of the primary antibody.[13]

Electron microscopic study

Small pieces (1 mm^3) from the lung were used for electron microscopy (EM). Specimens were immediately fixed in 2.5% glutaraldehyde for 24 h, washed in 0.1 M phosphate buffer at 4°C, and then postfixed in 1% osmium tetroxide at room temperature. Specimens were dehydrated in ascending grades of ethyl alcohol and then embedded in Epon resin. Semithin sections (1 μm) were stained with toluidine blue and examined with a light microscope. Ultrathin sections were cut, mounted on copper grids, and stained with uranyl acetate and lead citrate.[14] Specimens were examined and photographed with a JEM transmission EM in the EM Unit, Faculty of Medicine, Tanta University.

Quantitative and statistical study

Optical color intensity of caspase-3 immunoreactivity was estimated. The image analysis system (Leica Q 500 MC Program; Leica, Switzerland) in the Tanta Faculty of Medicine, Central Research Laboratory, Tanta, was used to measure the mean total optical density of caspase-3-positive immunoexpression.

Statistical analysis

The values were represented as mean ± standard deviation. The data were analyzed, calculated, and compared between groups using SPSS software for Windows, Version 11.0.1 (SPSS Inc., Chicago, Illinois, USA).

Results

No mortality occurred during the GNP administration periods, and no changes were observed in the appearance or behavior in treated rats versus the control rats.

Light microscopic results

Hematoxylin and eosin stain

Control group

Light microscopic examination of H and E-stained sections from control group revealed normal lung architecture with spongy structure, normal clear alveoli, and thin interalveolar septa [Figure 1].

Experimental groups

Variable histological changes were observed among the lung tissue of the experimental groups, both in pattern and severity. These changes were more severe in high dose than that in low-dose exposure to GNP. Sections from Group I (low-dose GNP) revealed loss of normal architecture of the lung tissue with thickening of interalveolar septa, collapse of some alveoli, and emphysematous dilation of the others [Figure 2]. Diffused inflammatory infiltrate within the interalveolar septa and focal around bronchioles was observed. As regard to changes in the bronchial wall, it showed vacuolation and desquamation of the lining epithelium with

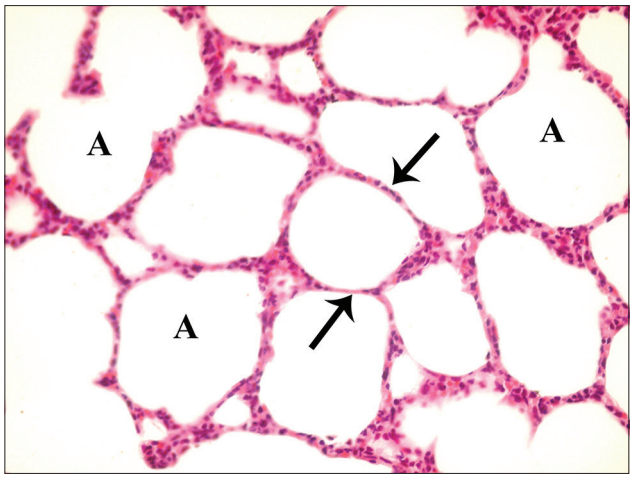

Figure 1: A photomicrograph of a lung section of control group showing normal lung architecture with spongy structure, normal clear alveoli (A), and thin inter-alveolar septa (arrow) (H and E, ×400)

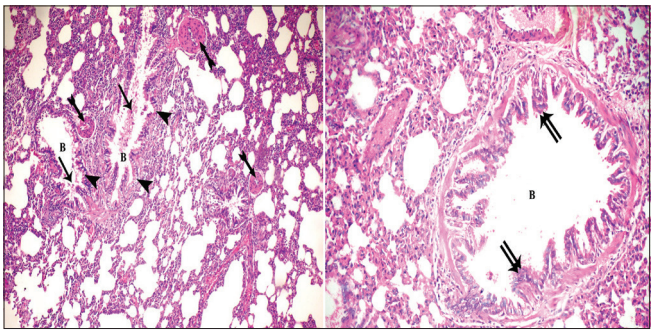

Figure 3: Photomicrographs of the lung sections of experimental Group I showing vacuolation (arrowhead) and desquamation of (arrow) the lining epithelium of some bronchioles (B) with focal increased thickness (double arrow) of others. Notice thick walled blood vessels (bifid arrow) (H and E, ×200, ×400)

focal increased thickness. Dilated congested blood vessels were detected [Figure 3].

In Group II (high-dose GNP), the lesions were increased, and the lung showed the pathological feature of pneumonia. The alveoli were full of cellular infiltrates as well as the interstitial tissue. Extravasated red blood cells (RBCs) were detected in the interalveolar spaces. Most of the alveoli became collapsed, and others became irregular air spaces [Figure 4]. Extravasated RBCs also observed in the lumen of the alveoli and some bronchioles and focal stratification of bronchial epithelium. In addition, dilatation and congestion of the blood vessels were severe [Figure 5]. There is also thickening of the intima and media. The media revealed spitting, edema, and disorganization of its layers with perivascular cellular infiltrate [Figure 6].

Immunostaining with caspase-3 antibodies

The positive reaction appeared as brown color in the cytoplasm of epithelial cells lining the alveoli of control group [Figure 7a]. An apparent increase in the reaction was detected in both Group I (low-dose GNPs) [Figure 7b]

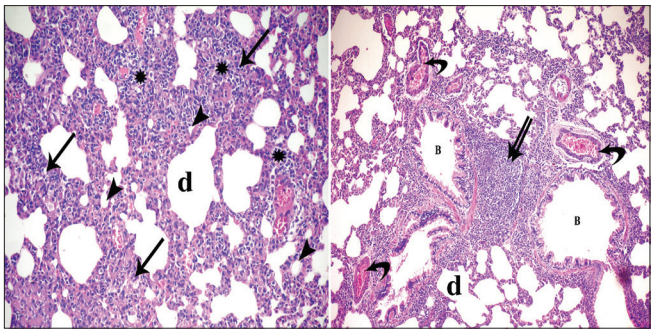

Figure 2: Photomicrographs of lung sections of experimental Group I showing loss of normal architecture of the lung tissue with thickening of interalveolar septa (arrow) and collapse of some alveoli (arrowhead) while other showing emphysematous dilatation (d). Diffused inflammatory infiltrates appear within the interalveolar septa (*) and focal (double arrow) in between the bronchioles (B). Notice dilatation and congestion of blood vessels (curved arrow) (H and E, ×400, ×200)

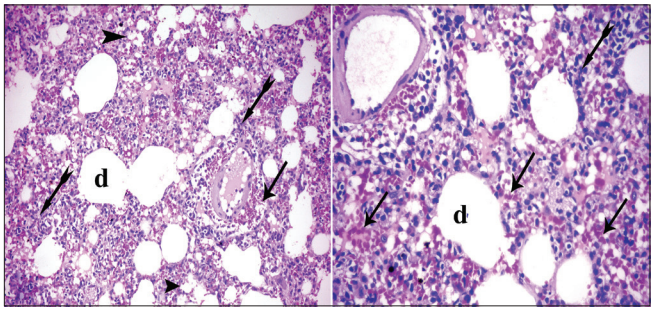

Figure 4: Photomicrographs of the lung sections of experimental Group II showing cellular infiltrates (bifid arrow) and the alveoli were full of cellular infiltrates and alveoli became collapsed (arrowhead); others became irregular air spaces (d). Extravasated red blood cells (arrow) in the interalveolar spaces as well as the interstitial tissue (H and E, ×200, ×400)

and Group II (high-dose GNPs) [Figure 7c]. The reaction was detected mainly around the blood vessels and involved inflammatory cells that infiltrated in the alveoli.

Statistical results

The optical density of caspase-3 immunoreactivity [Table 1 and Graph 1] showed that there was significant difference in the mean values of optical density of caspase-3 immunoexpression in all studied groups. There was a highly significant difference ($P < 0.000$) between the three studied groups; both low-dose GNP-treated group and high-dose GNP-treated group had highly significant increase as compared with control group.

Electron microscopic results

Control group

EM examination of the ultrathin lung sections of control group revealed patent alveoli with thin walls lined by flat pneumocyte type I which is the predominant cell type and cuboidal or dome-shaped type II pneumocytes with euchromatic nuclei and a few short microvilli on their cell surface. Their cytoplasm contained numerous lamellar bodies and multiple mitochondria [Figure 8].

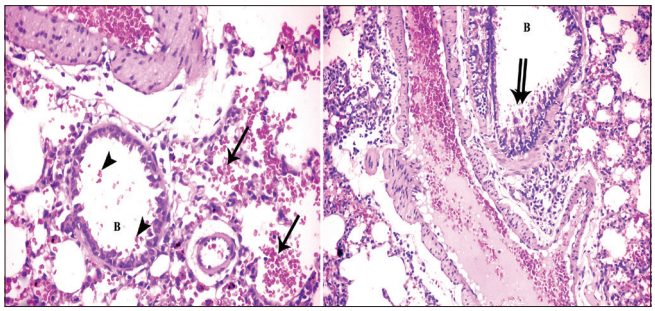

Figure 5: Photomicrographs of a lung section of experimental Group II showing extravasated red blood cells in lumen of the alveoli (arrow) and the bronchioles (B) (arrowhead) and focal stratification (double arrow) of bronchial epithelium. Notice dilated congested blood vessels (H and E, ×400, ×200)

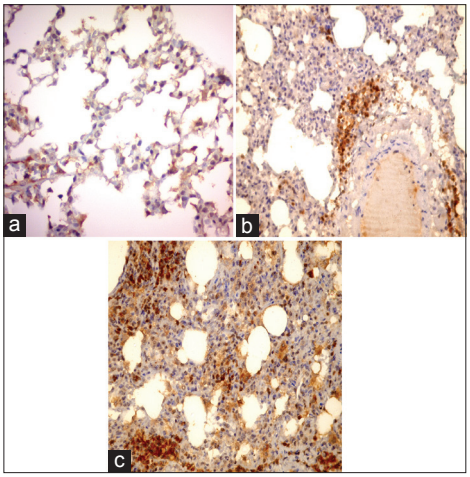

Figure 7: Photomicrographs of a lung section showing faint brown color in the cytoplasm of epithelial cells lining the alveoli of control group (a), an apparent increase in the reaction around the blood vessels (b), intense positive reaction and involve inflammatory infiltrates appear in Group II (c) Caspase-3 immunostaining, × 200

Experimental groups (Group I & Group II)

Group I (low dose of gold nanoparticles)

EMs of this group revealed alteration in the alveolar structure mainly type II pneumocytes that showed some degenerative changes of their lamellar bodies and mitochondria. Lamellar bodies appeared irregular, partially vacuolated, and decreased number and some were empty. As regard to mitochondria some of it appeared enlarged in size. In addition, nuclei of some pneumocytes type II showed indentation with condensed chromatin, others showed loss of their surface microvilli, while few cells were exfoliated in the alveolar lumen. Congested blood capillaries and collagen fibers were also observed [Figure 9].

Group II (high dose of gold nanoparticles) showed excessive inflammatory cellular infiltration. Type II pneumocytes were the predominant cells lining the alveoli that appeared collapsed with narrow alveolar lumen. Most of the pneumocytes showed mitochondria with variable degree of disrupted cristae. In addition, the interalveolar septum contains blood capillaries,

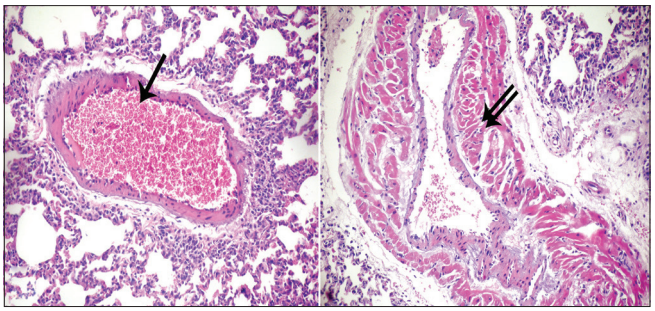

Figure 6: Photomicrographs of a lung section of experimental Group II showing dilated congested blood vessels (arrow) and other with thickened muscular wall (double arrow) (H and E, ×200)

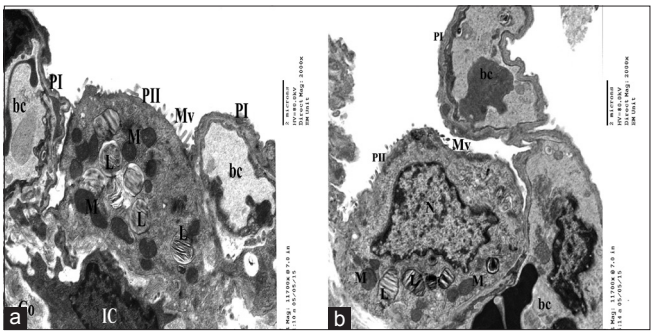

Figure 8: Electron micrographs of ultrathin section of control group showing a part of patent alveolus lined with type I pneumocyte (PI) and type II pneumocytes(PII) with few short microvilli(Mv) on the surface, (a) euchromatic nucleus(N), characteristic lamellar bodies (L) and multiple mitochondria(M) (b). The interalveolar septum contains blood capillaries (bc) interstitial cell (IC) and some collagen fibers (Co) (a&b)

Table 1: Optic density for caspase-3 immunostaining

Groups	Mean±SD	*P*
Control	29.872±5.37	-
Low-dose GNPs	58.1295±2.86	0.01
High-dose GNPs	72.2475±5.54	0

SD: Standard deviation, GNPs: Gold nanoparticles

interstitial cell, and some collagen fibers. Apparently, increased numbers of interstitial cells [Figure 10] and different inflammatory cells such as neutrophils, mast cells and lymphocytes, active fibroblast, and macrophages were also detected [Figure 11].

Discussion

GNPs showed vast growing multiple applications in nanomedicine, but its interaction with biological systems needs more study to evaluate its safety.

This work was done to see to what degree the NPs affect the lung tissue. The results of this work revealed severe alveolar damage in the form of collapsed alveoli, heavy infiltration in the lumen of alveoli, and interalveolar septa with inflammatory cells. This infiltrate composed mainly of macrophages and associated with congested blood capillaries and extravasations

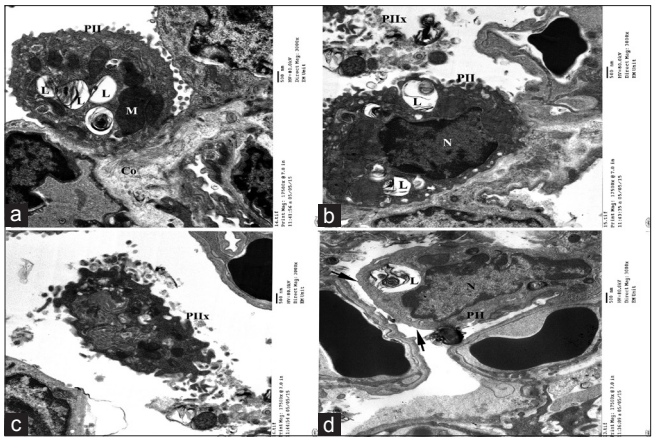

Figure 9: Electron micrographs of ultrathin section of experimental group I showing (a) type II pneumocyte (PII) lining the alveolar cavity with multiple empty lamellar bodies (L) and megamitochondria(M). (b) Nucleus of pneumocyte type II appears indented with electron dense chromatin. (c)Some pneumocyte type II exfoliated in the lumen (PIIx) and other showing blunt surface without microvilli (arrow). Notice congested blood capillaries (bc) (d) and collagen fibers (Co) (a)

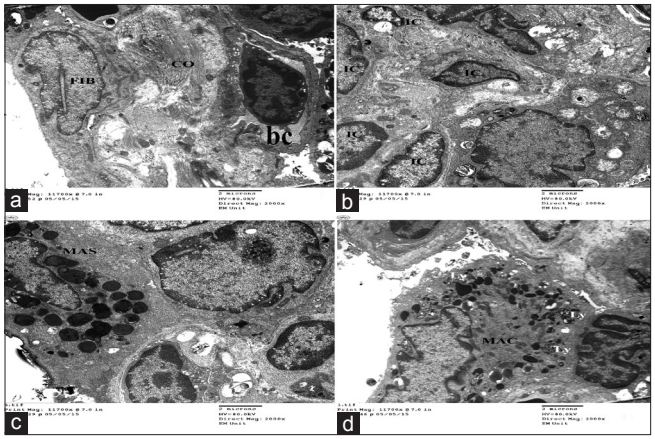

Figure 11: Electron micrographs of ultrathin section of experimental group II showing thick inter alveolar septa with deposition of excess collagen fibers associated with active fibroblast (FIB) with euochromatic nucleus (a) and apparent increased numbers of interstitial cells (IC) (b), different inflammatory cells like mast cells (MAS), and active macrophages (MAC) with excess electron dense bodies and secondary lysosome(Ly) (c&d). Notice blood vessels (bc) (a)

of RBCs. This infiltration was severe near the bronchioles and blood vessels. Ultrastructurally, proliferation of pneumocytes type II with degenerative changes in their lamellar bodies leaving irregular empty spaces was detected. In addition, active fibroblasts with collagen deposition were found mainly in Group III. The same finding was detected in other works in the form of perivascular and peribronchial neutrophilic and macrophage infiltration, shedding, and necrosis of the epithelium. These lesions were explained by oxidative damage induced by GNPs. This explanation was supported by ability of GNPs to induce oxidative stress in bronchial epithelia.[15,16] Furthermore, GNPs may cause damage of the epithelial cells leading to damaged respiratory barrier.[17]

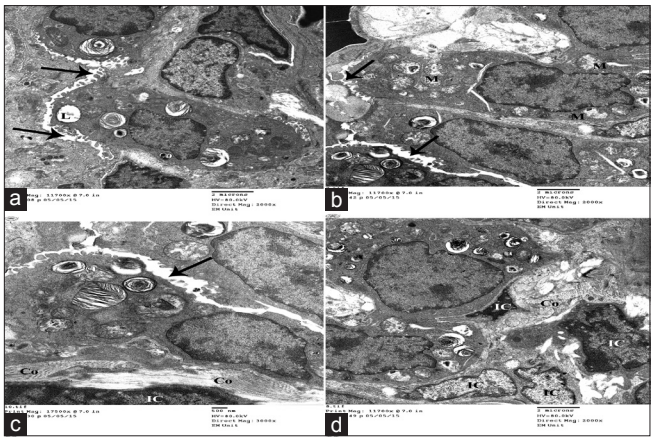

Figure 10: Electron micrographs of ultrathin section of experimental group II showing collapsed alveoli with very narrow alveolar space (arrow) (a). Type II pneumocytes is the predominant cell lining alveoli showing some empty lamellar bodies (L) and multiple mitochondria with disrupted cristae (M). (a-d) Inter alveolar septum contains more interstitial cells (IC) and collagen fibers (Co)(c and d)

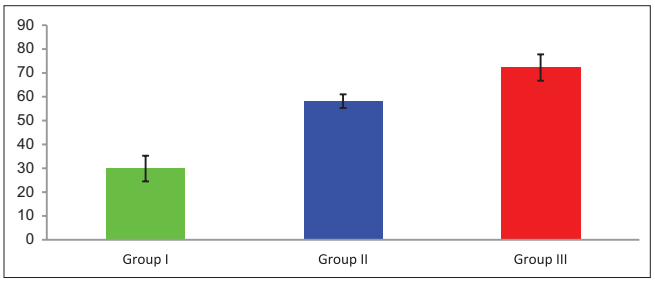

Graph 1: Mean Color intensity of caspase-3

Most prominent cells were activated macrophages and neutrophils as documented in previous works. Its pathogenesis depends on chemokines such as the cytokine-induced neutrophil chemoattractant and macrophage inflammatory protein-1α, leading to accumulation of neutrophil and macrophages in the affected lung. These macrophages help in removing the accumulated GNPs by their lysosomes.[18,19]

Cellular infiltrations with extravasations of RBCs in the lung tissue as well as diffuse interstitial pneumonia, fibrosis, and chronic inflammatory infiltrate were observed in this work. These changes could be due to interference with the antioxidant defense mechanism, leading to release of reactive oxygen species. Proteins and enzymes of lung tissue could also be affected.[20] Inflammation for prolonged time led to more damaging effect on the lung tissue as a result of release of free radicals and antioxidants. Fibrosis is the end result of these effects.[21,22]

Compressed air sacs and thickening of the air sacs wall were demonstrated in this work. This lesion was suggested as a result of imbalance between production and degradation of the surfactant. Increased thickness of the blood vessels wall and exfoliated cells in the lumen of the alveoli and in the bronchioles were prominent finding. All these observations might be related to the direct damaging effect of GNPs on

the lining epithelial. It induced epithelial damage to the respiratory barrier, which increased susceptibility of lung tissue to allergens as manifested by the presence of mast cells.[23,24]

Predominance of type II pneumocytes was manifested in this work. Some authors suggested that increased pneumocyte type II may be a compensatory for the damaged epithelial cells of the lung.[25]

Results observed by EM were in the form of increased type II pneumocytes with vacuolated abnormal-shaped lamellar body and degenerated mitochondria. These data were reported by other researcher. Vacuolations can be explained by disturbance in the function of membranes and increased entrance of sodium and water. Later, it results in swelling of the organelles. Further, lysosomal enzyme leakage leads to more degeneration. With regard to mitochondrial lesion, it related to change in its membrane potential, so it became swollen and degenerated.[1,26]

In relation to the immunohistochemical staining of caspase-3, there was significant increase in density of the stain in Group III more than Group II, this finding in accordance with the findings of Ding *et al*., and they documented that GNPs led to release of free radicals and an increase in apoptosis.[26]

In the same side, many authors reported that GNPs induced significant upregulation of mRNA expression of p53, bax, caspase-3, and caspase-9; these mediators increased apoptosis. Hence, apoptosis occurred through caspase-dependent mechanism.[27,28]

Lesions in Group II were less than that in Group III. These observations may be due to dose and duration of exposure to GNPs.[29] Since uptake of GNPs occurs through two phases. Rapid phase starts for few hours after intake then enters in plateau phase after 6 h. The plateau phase occurred as a result of serum proteins binding to the surface of GNPs ending in GNP–protein complex which is more stable than free form of GNPs.[30]

Uptake of GNPs affected by its size where GNPs up to 200 nm depended on clathrin-mediated endocytosis, while large particles need other method to enter the cells.[31] General mechanisms of GNPs depend on induction of inflammation and production of free radicals in the form of reactive oxygen and nitrogen species. These radicals lead to DNA and proteins damage.[32,33]

Conclusions

These results indicated that GNPs produced injurious histological changes on the lung tissue. Further investigations on the effect of GNPs on different tissues are needed.

Acknowledgments

I would like to thank Dr. Awatiff EL-Shall, Professor of Histology, Faculty of Medicine, Tanta University, for her help and support.

Financial support and sponsorship

Nil.

Conflicts of interest

There are no conflicts of interest.

References

1. Abdelhalim MA. Uptake of gold nanoparticles in several rat organs after intraperitoneal administration *in vivo*: A fluorescence study. Biomed Res Int 2013;2013:353695.
2. Sung JH, Ji JH, Park JD, Song MY, Song KS, Ryu HR, *et al.* Subchronic inhalation toxicity of gold nanoparticles. Part Fibre Toxicol 2011;14:8-16.
3. Song Y, Li X, Du X. Exposure to nanoparticles is related to pleural effusion, pulmonary fibrosis and granuloma. Eur Respir J 2009;34:559-67.
4. Ghosh P, Han G, De M, Kim CK, Rotello VM. Gold nanoparticles in delivery applications. Adv Drug Deliv Rev 2008;60:1307-15.
5. Cheng Y, Samia AC, Meyers JD, Panagopoulos I, Fei B, Burda C, *et al.* Highly efficient drug delivery with gold nanoparticle vectors for *in vivo* photodynamic therapy of cancer. J Am Chem Soc 2008;130:10643-7.
6. MacNee W, Donaldson K. Mechanism of lung injury caused by PM10 and ultrafine particles with special reference to COPD. Eur Respir J Suppl 2003;40:47s-51s.
7. Kogan MJ, Olmedo I, Hosta L, Guerrero AR, Cruz LJ, Albericio F, *et al.* Peptides and metallic nanoparticles for biomedical applications. Nanomedicine (Lond) 2007;2:287-306.
8. Mansour HM, Rhee YS, Wu X. Nanomedicine in pulmonary delivery. Int J Nanomedicine 2009;4:299-319.
9. Schulz F, Homolka T, Bastús NG, Puntes V, Weller H, Vossmeyer T, *et al.* Little adjustments significantly improve the turkevich synthesis of gold nanoparticles. Langmuir 2014;30:10779-84.
10. Kara Z, William G, Sanjeev K, Marie-Christine D. Effect of high gold salt concentrations on the size and polydispersity of gold nanoparticles prepared by an extended Turkevich-Frens method. Gold Bull 2012;45:203-11.
11. Lasagna-Reeves C, Gonzalez-Romero D, Barria MA, Olmedo I, Clos A, Sadagopa Ramanujam VM, *et al.* Bioaccumulation and toxicity of gold nanoparticles after repeated administration in mice. Biochem Biophys Res Commun 2010;393:649-55.
12. Gample M. The hematoxylin and eosin. In: Bancroft D, Gamble M, editors. Theory and Practice of Histological Techniques. 6th ed., Ch. 9. China: Elsevier; 2008. p. 121.
13. Ramos-Vara JA, Kiupel M, Baszler T, Bliven L, Brodersen B, Chelack B, *et al.* Suggested guidelines for immunohistochemical techniques in veterinary diagnostic laboratories. J Vet Diagn Invest 2008;20:393-413.
14. Kuo J. Electron Microscopy, Methods and Protocols. 2nd ed. Totowa, New Jersey: Humana Press Inc.; 2007. p. 369.
15. Pan Y, Leifert A, Ruau D, Neuss S, Bornemann J, Schmid G, *et al.* Gold nanoparticles of diameter 1.4 nm trigger necrosis by oxidative stress and mitochondrial damage. Small 2009;5:2067-76.
16. Hussain S, Vanoirbeek JA, Luyts K, De Vooght V, Verbeken E, Thomassen LC, *et al.* Lung exposure to nanoparticles modulates an asthmatic response in a mouse model. Eur Respir J 2011;37:299-309.
17. Ruenraroengsak P, Novak P, Berhanu D, Thorley AJ, Valsami-Jones E, Gorelik J, *et al.* Respiratory epithelial cytotoxicity and membrane damage (holes) caused by amine-modified nanoparticles. Nanotoxicology 2012;6:94-108.
18. Desouza IA, Hyslop S, Franco-Penteado CF, Ribeiro-DaSilva G. Mouse macrophages release a neutrophil chemotactic mediator following stimulation by staphylococcal enterotoxin type A. Inflamm Res 2001;50:206-12.
19. Morimoto Y, Izumi H, Kuroda E. Significance of persistent inflammation in respiratory disorders induced by nanoparticles. J Immunol Res 2014;2014:962871.
20. Tedesco S, Doyle H, Blasco J, Redmond G, Sheehan D. Oxidative stress and toxicity of gold nanoparticles in mytilus edulis. Aquat Toxicol 2010;100:178-86.
21. Ogami A, Morimoto Y, Myojo T, Oyabu T, Murakami M, Nishi K, *et al.* Histopathological changes in rat lung following intratracheal instillation of silicon carbide whiskers and potassium octatitanate whiskers. Inhal

Toxicol 2007;19:753-8.
22. Morimoto Y, Izumi H, Yoshiura Y, Fujishima K, Yatera K, Yamamoto K, *et al*. Usefulness of intratracheal instillation studies for estimating nanoparticle-induced pulmonary toxicity. Int J Mol Sci 2016;17. pii: E165.
23. Devalia JL, Rusznak C, Davies RJ. Allergen/irritant interaction – Its role in sensitization and allergic disease. Allergy 1998;53:335-45.
24. Abdelhalim MA, Jarrar BM. Gold nanoparticles administration induced prominent inflammatory, central vein intima disruption, fatty change and kupffer cells hyperplasia. Lipids Health Dis 2011;10:133.
25. Durmuş-Altun G, Altun A, Aktas RG, Salihoglu YS, Yigitbasi NO. Use of iodine-123 metaiodobenzylguanidine scintigraphy for the detection of amiodarone induced pulmonary toxicity in a rabbit model: A comparative study with technetium-99m diethyltriaminepenta acetic acid radioaerosol scintigraphy. Ann Nucl Med 2005;19:217-24.
26. Ding F, Li Y, Liu J, Liu L, Yu W, Wang Z, *et al*. Over endocytosis of gold nanoparticles increases autophagy and apoptosis in hypoxic human renal proximal tubular cells. Int J Nanomedicine 2014;9:4317-30.
27. Selim ME, Hendi AA. Gold nanoparticles induce apoptosis in MCF-7 human breast cancer cells. Asian Pac J Cancer Prev 2012;13:1617-20.
28. Noël C, Simard JC, Girard D. Gold nanoparticles induce apoptosis, endoplasmic reticulum stress events and cleavage of cytoskeletal proteins in human neutrophils. Toxicol *In Vitro* 2016;31:12-22.
29. Jong WH, Burger MC, Verheijen MA, Geertsma RE. Detection of the presence of gold nanoparticles in organs by transmission electron microscopy. Materials (Basel) 2010;3:4681-94.
30. Chithrani BD, Ghazani AA, Chan WC. Determining the size and shape dependence of gold nanoparticle uptake into mammalian cells. Nano Lett 2006;6:662-8.
31. Kreyling WG, Semmler-Behnke M, Möller W. Ultrafine particle-lung interactions: Does size matter? J Aerosol Med 2006;19:74-83.
32. Kliment CR, Oury TD. Oxidative stress, extracellular matrix targets, and idiopathic pulmonary fibrosis. Free Radic Biol Med 2010;49:707-17.
33. Jin C, Tang Y, Yang FG, Li XL, Xu S, Fan XY, *et al*. Cellular toxicity of TiO2 nanoparticles in anatase and rutile crystal phase. Biol Trace Elem Res 2011;141:3-15.